Original article

A.K. Vasudevan*, K. Sadananda and P.S. Pao

Residual stress affecting environmental damage in 7075-T651 alloy

https://doi.org/10.1515/corrrev-2019-0018
Received January 7, 2019; accepted March 1, 2019; previously published online June 22, 2019

Abstract: The role of tensile overload superimposed on a constant amplitude cycling results in compressive residual stresses at the crack tip that cause crack growth retardation. The degree to which this effect manifests depends on whether the tests are done at a constant driving force (K_{max}) or at a constant crack growth rate (da/dN). It is observed that depending on the magnitude of the overload at a given applied base stress intensity, these residual stresses can have significant effect on the crack growth in both the inert (vacuum) and the chemical (NaCl) environments. In general, cracks will grow only if the total crack tip driving force K_{total} exceeds the long crack intrinsic threshold $K^*_{max,th}$. The crack growth retardation results can be attributed to the combined effects of the crack tip chemical reaction rates and the overload compressive residual stresses.

Keywords: Driving force DK & K_{max}; overload residual stress; Kitagawa diagram.

1 Introduction

Structural components during service experience random variable load amplitudes that can be tensile and compressive. Such random loads affect the overall life cycle of the component. Tensile overloads result in compressive residual stress that retards the crack growth, while the compressive overloads add tensile residual stress that accelerates the growth. If in addition, an aggressive chemical environment is superimposed during underloads or overloads, then the damage can accelerate or decelerate. Thus, variable loads along with superimposed environment affect the total life of a component in service.

Causes and effects of crack retardation and acceleration due to variable amplitude loads have been studied earlier and described by Suresh (1998) who attributed them to several factors such as crack closure, crack deflection, residual stress, strain hardening and crack branching/blunting. Later, detailed analysis on the role of these variable loadings on damage has been re-examined by Sadananda et al. (1999), Sadananda and Vasudevan (2004) pointing out that the role of residual stress generated by these loads is more significant than the reasons listed by Suresh (1998).

To date, the studies on the effect of environment during fatigue has been focused mainly towards understanding the changes in the crack growth rates (da/dN) at a constant applied crack tip driving force K than the role of the crack driving forces. This is understandable as the life prediction methods require periodic non-destructive damage inspections of cracks formed during service as there is an uncertainty in predicting the crack growth variations due to the environment, which is always present during service. Hence, less attention is given to the role of the crack driving force on the damage.

This article attempts to characterize and understand the driving forces that affect retardation (or acceleration) of cracks due to overload (or underloads) and the role of chemical environment in accentuating these effects. Here we are comparing the role of overloads during a background of constant amplitude (CA) loading in a vacuum vs. an aggressive environment. In order to understand the chemical and mechanical driving forces affecting crack initiation and growth, we examine the variations in the applied K with the crack extension due to overloads in the presence of an environment. Unfortunately, the changes in the crack tip chemistry due to stress changes are not well documented or understood, and there is a lack of appropriate fractographic data. As a result, we assume that the crack tip chemistry remains constant during these stress changes. In short, we are studying how the

***Corresponding author: A.K. Vasudevan,** Technical Data Analysis, Inc., 3190 Fairview Park Drive, Suite 650, Falls Church, VA 22042, USA, e-mail: akruva@gmail.com
K. Sadananda: Technical Data Analysis, Inc., 3190 Fairview Park Drive, Suite 650, Falls Church, VA 22042, USA
P.S. Pao: Naval Research Laboratory (Retired), Washington, DC 20375-5320, USA

overloads affect the steady state crack growth behavior in two different environments (vacuum and NaCl) and compare their results. This study is not related to the overload-environment interactions.

To accomplish this, a study is made using 7075-T651 alloy, which is subjected to a single overload (OL ~ 300%) followed by the CA fatigue cycling, at a given load ratio (R = 0.1), in a vacuum (~10^{-8} torr) and in 1% NaCl, pH = 4 solution. These two environments remain constant during the CA and OL tests. The 7075-T651 alloy was selected because of its environmental susceptibility in NaCl solution. Thus, keeping the alloy composition and the environmental composition constant with a single application of an OL gives the simplest case to analyze the crack growth retardation behavior.

2 General concepts

Components in service are subjected to dynamic mechanical loads and chemical environments. Hence, one must characterize the mechanical and chemical contributions to damage. We can only measure mechanical properties in terms of stress/cycle or (da/dN)-K_{max} and observe how chemistry helps augment the driving force to failure. Characterization involves applied stresses with and without the presence of a chemical environment. We then define an inert environment data as a reference to quantify the role of chemistry on damage. Next, we introduce the concept of "internal stress" in inert environment generated by plasticity due to mechanical loads and that in chemical environments due to chemical potential gradients. Chemical internal stresses can decrease or increase plasticity depending on the extent of the crack tip chemical reaction.

Cyclic loading in an inert environment generates local plasticity to generate "internal stresses" that can help the applied stresses to meet the threshold conditions to form a crack and grow. In a chemical environment, chemical potential gradients establish chemical forces that are specific to the material-environment system, and they depend on the details of the crack tip chemical reactions. The chemical force reduces the applied stress by reducing the surface energy of the material without any knowledge of the mechanism. We use inert environment as a reference state to define the chemical forces as resulting in "chemical internal stress". Since we measure only the mechanical forces, we termed the chemical effects as a "mechanical equivalent of chemical force" to describe its effect on the crack extension. Chemical stress is measured by the reduction in the mechanical forces required to initiate and propagate a crack in that material-environment system.

Environmental contribution reduces the applied stresses to provide the same material response or can enhance the crack growth rate for the same applied mechanical force. This is a very brief description from the several articles by Sadananda et al. (2001, 2017), Sadananda and Vasudevan (2011), Sadananda (2012) where detailed analysis is presented.

Thus, the description for a crack to nucleate and grow involves the following:

1. Applied stresses generating plasticity giving a "mechanical internal stress";
2. Chemistry helping to reduce the applied stresses, given by "chemical internal stress";
3. Overall effect is to change the material resistance or its response to form a crack and grow; and
4. In the absence of an environment one can generalize: $K_{appl} \pm K_{int} > K^{*}_{max,th}$.

3 Method of analysis

To date, there are two types of experiments that can be used to characterize the environmental damage in materials. These are stress-controlled (S-N fatigue) using a smooth or notched tensile sample where stress varies with number of cycles (N_f). The other is a fracture mechanic sample where the crack length is measured with the number of cycles. Since corrosion fatigue is time and cycle dependent, frequency of loading is a common factor to be considered in these experiments to characterize the data. Varying the frequency for a given environment and applied driving force is a common method to characterize the material response in terms of N_f or (da/dN). As a result, work on the role of applied stress affecting the damage has been less emphasized since the applied frequency must be very low (<0.01 Hz for a 7075-T6 alloy in 3% NaCl) to observe the time effects on damage. That requires very long time tests.

Since environment affects both the applied crack tip driving force and the resulting crack growth rates, we can define two methods to characterize fatigue damage. One method is to characterize the material response [like cycles to failure N_f or (da/dN)] and the other is the driving force (like applied stress $\Delta\sigma$ and σ_{max} or stress intensity ΔK and K_{max}) in each environment. This can be done in a stress-controlled S-N fatigue or using a fracture mechanics (da/dN)-K_{max} or ΔK method. Both give similar trends in behavior. The former method gives information on crack nucleation, and the later addresses crack growth.

To illustrate the above methods, we first examine the behaviors in a stress-controlled S-N fatigue (stress-N_f

cycles) under the influence of a chemical environment, in a CA cycling. Our reference curves, S-N or (da/dN)-K_{max}, is the inert (vacuum) environment. Figure 1A shows schematically S-N fatigue behavior in inert and aggressive environments. Note that the S-N curve is lower in the aggressive environment compared to the inert. At a given N_f cycle, stress in the inert environment is reduced by the chemical environment or at a given stress $\Delta\sigma$, N_f is reduced by the environment to cause failure. These variations affect the S-N behavior of the inert environment as follows: (1) reduction in N_f at a constant stress $\Delta\sigma$ and (2) reduction in stress $\Delta\sigma$ at a constant N_f. Thus, the effect of environment can thus be described in these two ways as (1) reduction in the stress to cause failure for a given number of cycles or (2) reduction in the number of cycles to failure for a given applied stress.

Similar behavior can be observed for the case of CA fatigue crack growth (FCG) behavior, shown schematically in Figure 1B. Here the environment lowers the applied crack driving force resulting in increased crack growth rates, moving the entire environmental FCG curve to the left of the vacuum. These descriptions are shown in Figure 1B as crack growth rates FCG-1 and 2 representing (1) at constant (da/dN) and (2) at constant applied K_{max}. Thus, the effect of the environment on the crack growth can also be described in two ways: (a) change in the applied crack tip driving force to enforce the same crack growth rates (Type-A) or (b) change in crack growth rates due to the environment for the same applied crack tip driving force (Type-B). At points A (vacuum), B (NaCl) and C (NaCl) a single 300% OL is applied followed by CA loading at R = 0.1 to characterize the post overload (Post-OL) FCG behavior, shown in Figure 1B with the vacuum as the reference state. Figure 1C shows the details of the experimental methods for the discussion.

Using Figure 1C, we can define few parameters that can help characterize the mechanical and chemical driving forces as a: this is leading to the list of small equations (1) through (8).

Mechanical driving force K is the difference between K_{appl} and $\pm K_{res}$ (due to overload or underload) for each environment and at any FCG value. In the present case, since we apply a single OL, $K_{res} < 0$. K_{appl} is the same as K_{base} from which a single OL of 300% is applied.

$$\text{In the vacuum with no NaCl, } K_{vac} = K_{mech} = K_{app,vac} - K_{res,vac} \tag{1}$$

The total crack tip driving force in a vacuum is due to the mechanical contribution to K:

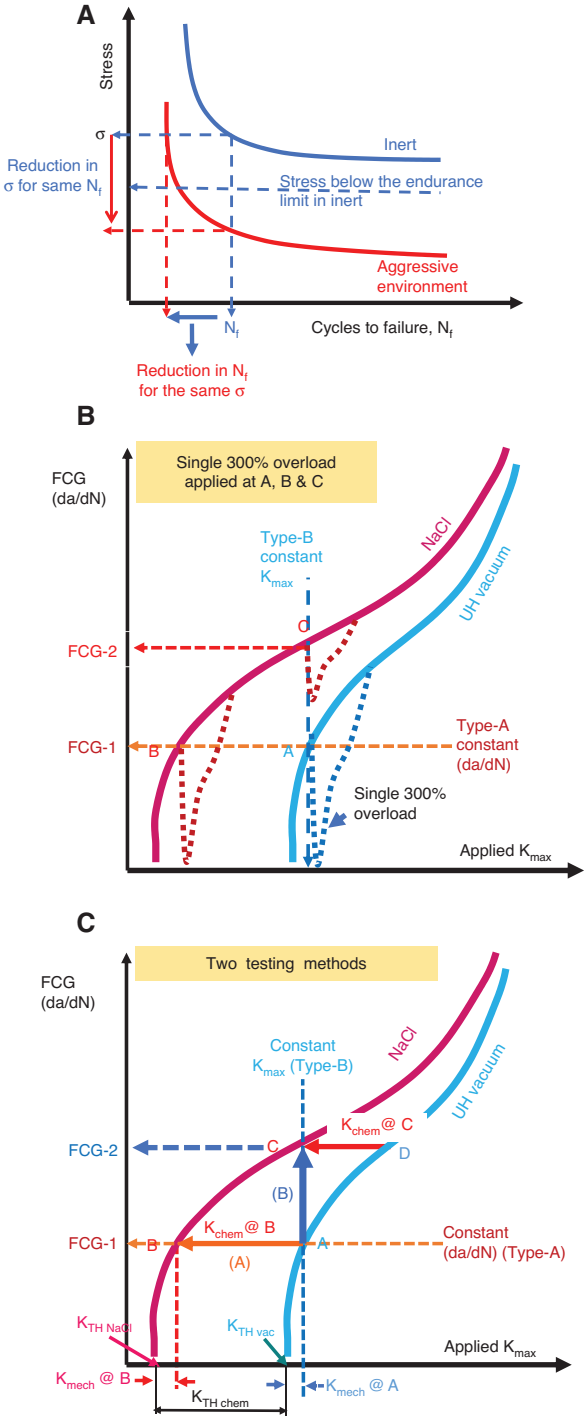

Figure 1: Schematic illustration showing that the environment affects both crack tip driving force and the crack growth rates under constant amplitude loading for S-N fatigue (A) and for FCG (B). Two possible descriptions can be used to define the environmental effects: (a) decrease in applied stress at a constant response N_f or (da/dN) or (b) decrease in N_f or (da/dN) at a constant applied stress $\Delta\sigma$ or K_{max}. Figure 1B gives all the necessary parameters needed for analysis. In Figure 1B, a single 300% overload is applied at points A, B and C; Figure 1C shows the detailed K-parameters from Figure 1B and is listed in the text.

$$K_{tot,vac} = K_{mech} \quad (2)$$

The chemical driving force at a given (da/dN) is the chemical contribution to K as follows:

$$K_{chem} = K_{appl,vac} - K_{appl,NaCl} (@\,\text{FCG-1 and 2}) \quad (3)$$

For the present case,

$$K_{NaCl}(@\text{FCG-1}) = K_{Vac}(@\text{A}) - K_{NaCl}(@\text{B}) \quad (4)$$

$$K_{NaCl}(@\text{FCG-2}) = K_{Vac}(@\text{D}) - K_{NaCl}(@\text{C}) \quad (5)$$

The total crack tip driving force in NaCl

$$K_{tot,NaCl} = K_{appl,NaCl} - K_{res,NaCl} + K_{chem} \quad (6)$$

The minimum chemical force is at threshold

$$K_{TH,chem} = K_{TH,vac} - K_{TH,NaCl} \quad (7)$$

(assuming K_{res} in both environments is negligible)

$$\text{Cracks will grow if } K_{total} > K^*_{max,th} \quad (8)$$

Equation (8) applies for both the vacuum and NaCl environments.

The contributions from Eq. (4) are small, because the CA-FCG (log-scale) curve dips towards K_{TH}; for FCG-1 see Figure 1C. It should be noted that Figure 1C is all in applied K_{max}. The contributions are however large at the higher FCG-2. Using Figure 1B and C, we can describe two methods of analysis:

1. Type-A defines the changes in the crack tip driving force (ΔK or K_{max}) at a *constant crack growth rate* (da/dN). In this case, the forces include both applied mechanical stresses and those due to the crack tip chemical driving forces. Chemical force is reducing the applied K_{max} since the response (da/dN) is kept constant. The latter depends on the type of chemical reaction processes that are involved at the crack tip. This method helps in distinguishing the contribution of chemical versus mechanical forces.
2. Type-B defines the increase in the crack growth rates for a *constant applied driving force* (K_{max}) and attributes the (da/dN) change to the influence of the environment. Here the response (da/dN) is used to define the chemical force contribution to the damage. That is, the same material response is assumed for the applied K_{max} and acting chemical force. This method gives information about the change in the kinetics of the environmentally induced crack growth for a selected applied mechanical driving force. Here we can obtain additional increment in the crack growth due to the superimposed environmental contributions.
3. In many cases, if the thresholds are significantly reduced by the environment, the crack growth rates for the same applied K_{max} by Type-B can be difficult to define due to some overlap in the FCG curves. On the other hand, one can always define, using the method in Type-A, to characterize the change in the crack tip driving forces at any crack growth rate.
4. Type-A can be viewed as a contribution from mechanical forces while Type-B as due to chemical forces. Given such a description, it is possible to quantify and characterize the material response in a given environment (like NaCl) in relation to an inert environment (like a vacuum).

4 Material properties and experimental design

The environment can affect the fatigue crack growth depending on the applied K_{max} value being less or greater than the stress corrosion (SCC) threshold K_{Iscc}. Based on this observation, corrosion-assisted fatigue crack growth behavior was classified into three types and was discussed in detail in one of our early articles by Vasudevan and Sadananda (1995). In all three cases considered the SCC threshold was considered to be greater than the fatigue thresholds ($K_{Iscc} > K_{max,th}$) for a given R ratio. Since SCC is both stress and time dependent, frequency dependence on stress-corrosion fatigue can become noticeable when applied K_{max} is less or greater than K_{Iscc}. The corrosion fatigue in an aggressive environment was compared to the crack growth in an inert (vacuum) environment and is classified as time-dependent (frequency is important), stress-dependent and stress-time-dependent processes. This classification can be extended to the Post-OL FCG region which is under CA cycling.

Alloy selected for study is a precipitation-hardened 7075-T651 aluminum alloy that was heat treated to give yield stress (σ_{ys}) = 505 MPa, tensile stress = 575 MPa and fracture toughness $K_{Ic} \sim 22$ MPa(m)$^{1/2}$. Fatigue tests were conducted using pre-cracked standard compact tension (CT) sample of 12.7 mm thickness in S-T direction. The standard CA fatigue crack growth behavior [(da/dN) vs. K_{max}] was recorded at R = 0.1 (Figure 2A) in a 4×10^{-8} torr vacuum and in 1% NaCl at pH = 4. At R = 0.1 $K_{max} \sim \Delta K$ and vary by ~10%. Frequency of loading was 5 Hz for NaCl test and 10 Hz for the vacuum, at room temperature.

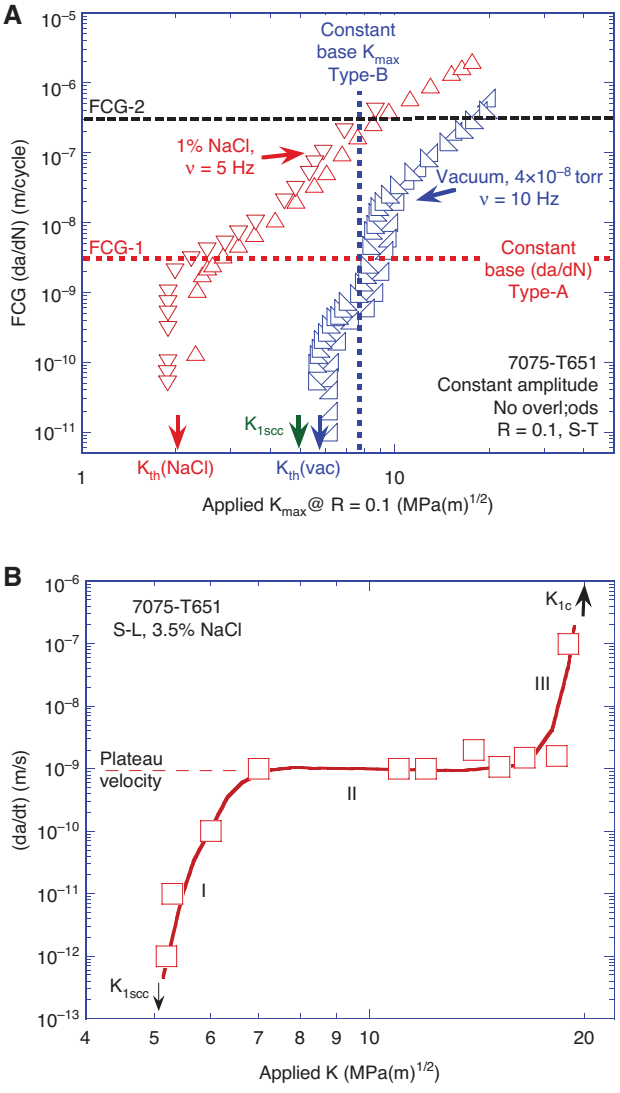

Figure 2: (A) Standard experimental constant amplitude fatigue crack growth data at R = 0.1 in the vacuum and in the NaCl solution, for 7075-T651 alloy from two different Navy labs. The key experimental features are shown defining the two types of tests; (B) the comparison experimental static SCC curve (da/dt)-K curve for 7075-T651 with three regions of crack growth.

Since environmental fatigue is frequency dependent, Mason (1994) has shown that for 7075-T651 alloy at ΔK (applied) = 9 and 15 MPa(m)$^{1/2}$ (da/dN) did not change much with frequency from 50 Hz down to 0.01 Hz in a 2.5 NaCl +0.5 Na_2CrO_4, pH = 3 aqueous solution. Similarly, Chanani (1976, 1978) also observed in 7075-T6 alloy that frequency change between 0.5 Hz and 15 Hz in 3.5% NaCl had negligible effect on the crack growth for this single OL + CA cycling experiment (Chanani, 1975). He also measured crack closure after single OL and found it to have insignificant effect but stated that OL plastic zone size (PZS) affected the retardation delay cycles during the crack growth. Such observations suggest the present FCG results conducted in the frequency range of 1–10 Hz is more frequency dependent than time at R = 0.1.

Figure 2A represents the experimental CA FCG curves (da/dN-K_{max}) for the vacuum and NaCl environments where the crack velocity varies with the applied K_{max}. NaCl decrements the applied K_{max} and increases (da/dN), shifting the NaCl curve to lower K_{max} level with respect to the vacuum. The CA threshold $K_{max,th}$ was about 5.9 MPa(m)$^{1/2}$ in the vacuum and 1.9 MPa(m)$^{1/2}$ in NaCl, respectively, at R = 0.1. Variation in the intrinsic threshold $K^*_{max,th}$ for the 7075-T651 alloy in the vacuum is about 5.5–6.1 MPa(m)$^{1/2}$, and that for NaCl is about 1.0–1.2 MPa(m)$^{1/2}$ (Pao & Holtz, 2014). At FCG-1 for Type-A, applied $K_{max} < K_{1scc}$ suggests that no SCC cracking occurs and yet the corrosion environment affects fatigue damage. This is the true corrosion fatigue which is time dependent. At higher growth rates ~10^{-7} m/cycle, FCG-2 for Type-B, applied $K_{max} > K_{1scc}$ indicates a stress-induced corrosion crack growth is superposed on the FCG process. It is noted that there was no observable plateau in the NaCl-FCG curve at the higher crack growth rates. A plateau at higher FCG is indicative of an H-type transport cracking mechanism, commonly seen in steels. Environmental contribution from NaCl can be estimated by using Eq. (4) or (5):

$$K(\text{environment}) = K(\text{chem}) = K(\text{vacuum}) - K(\text{NaCl})$$
at a constant FCG.

Figure 2B shows the static load SCC result for the same alloy in 3.5% NaCl, as (da/dt)-K, showing the three Stages (I, II and III) of SCC. In each stage the cracking is governed by different chemical processes. In Stage-I, it is thought that it is the rate of chemical reaction at the crack tip that determines the crack velocity. In this region, the crack velocity is stress dependent; factors governing the K-independent Stage-II are controlled by the kinetics of diffusion of some ions to the crack. In Stage-III, the applied K is high approaching K_{1c} [= 22 MPa(m)$^{1/2}$], and fracture occurs before any significant chemical reaction can occur. For 7075-T651 alloy the SCC-threshold in Stage-I for 3.5% NaCl is K_{1scc} ~ 5 MPa(m)$^{1/2}$.

Following the description in Figures 1B and C and 2A, the experimental design is constructed mainly into two parts with descriptions pertaining to Figure 2A:

1. In Type-A (points A and B, Figure 1C) experiment, at a *constant applied fatigue crack growth rate* (da/dN) = 3×10^{-9} m/cycle = FCG 1 there are two differing *applied* K_{max}. One at applied $K_{max} = K_{base} = 2.8$ MPa(m)$^{1/2}$ for 1% NaCl and the other at

$K_{base} = 7.9$ MPa(m)$^{1/2}$ for the vacuum. This experiment is done at (da/dN) close to the near-threshold region in CA. Applied $K_{base}(NaCl) << K_{base}(vacuum)$ (Figure 2A). Here $K(env) = K_{chem}$ @ B ~ 5.1 MPa(m)$^{1/2}$ at FCG-1. When a single 300% OL was applied, cracking was arrested for both the NaCl and vacuum environments, and the threshold shifted to 3.6 MPa(m)$^{1/2}$ for NaCl and 10.5 MPa(m)$^{1/2}$ for the vacuum. This, in the Post-OL region $K_{chem} = 6.9$ MPa(m)$^{1/2}$, was constant with the crack extension. Thus, for Type-A experiment, both K_{chem} and (da/dN) are constant.

2. In the Type-B (points A and C, Figure 1C) experiment with *constant applied driving force* K_{max} for the vacuum and NaCl, *applied* $K_{max} = 7.9$ MPa(m)$^{1/2}$; the $(da/dN) = 3 \times 10^{-9}$ m/cycle is at FCG-1 for the vacuum and is lower by 2 orders of magnitude compared to 1% NaCl$(da/dN) = 3 \times 10^{-7}$ m/cycle at FCG-2, and threshold remained at ~7.9 MPa(m)$^{1/2}$. At FCG-2, $K(env) = K_{chem}$ @ C ~ 10.5 MPa(m)$^{1/2}$ under CA loading. When 300% OL was applied in NaCl, cracking was not arrested, but (da/dN) decreased by 2 orders to $\sim 8 \times 10^{-10}$ m/cycle, and the crack began growing under Post-OL CA loading. However, the same OL arrested the crack in the vacuum and shifted the threshold to 10.5 MPa(m)$^{1/2}$. After the application of OL at C (Figure 1C), (da/dN) reduced to a minimum $\sim 8 \times 10^{-10}$ m/cycle where $K_{max} \sim 7.9$ MPa(m)1/2. The corresponding vacuum $K_{max} \sim 10.5$ MPa(m)1/2 and $K_{chem} \sim 2.6$ MPa(m)$^{1/2}$. Thus, for Type-B case, K_{chem} component increased with the crack growth, from about 2.6 to 14.6 MPa(m)$^{1/2}$, but the applied $K_{max} = K_{base}$ is kept constant.

The crack growth properties for the CT sample under these two conditions is monitored by measuring the load and crack extension using a potential drop method and the stress intensity (K) estimated by using the equations from Dowling (1993):

$$K = F_P P / t\,(b)^{0.5} \text{ with } P = \text{load}, t = \text{thickness and}$$
$$b = \text{width of the sample; and}$$
$$F_P = [(2+\alpha)/(1-\alpha)^{1.5}] \cdot \{0.886 + 4.64\,\alpha - 13.32\,\alpha^2 + 14.72\,\alpha^3 - 5.6\,\alpha^4\}$$

where $\alpha = a/b$, a = crack length from the loading line, b = sample width.

For the center crack sample: $F_P = \{1.297 - 0.297 \text{ Cos } (\pi\alpha/2)\}/(\sin \pi\alpha)^{1/2}$.

The above section gives the details of the experimental setup in CA and in static load conditions. It also describes the experimental parameters for the vacuum and NaCl environments needed for OL experiments.

4.1 Single overload experiments

The schematic illustration in Figure 3 shows the load sequence events that occur when a single OL is superimposed on CA cycles at R = 0.1 with changes in cyclic and monotonic PZS. The retardation is commonly measured in terms of delay cycles, N_d, before the original steady state CA conditions are re-established; see insert in Figure 3. N_d depends on background PZS at a K_{base} and the OL-PZ sizes. All factors that influence the plasticity at the cracktip will also have a direct effect on OL retardation (Sadananda et al., 1999). During CA cycles, prior to OL application, the PZS has a cyclic PZ imbedded in a larger monotonic PZ. When the OL is applied at a K_{base}, the monotonic PZ enlarges keeping the prior CA-PZ within. It is just OL-PZ that gives the retarding force on the crack tip which is more than the CA-PZ (dotted) that results in the excess effect that is considered as a compressive residual stress. This residual stress causes a reduction in the crack tip driving force that influences the subsequent crack extension. This is schematically shown as a smaller CA-PZ (dotted line at K_{base}) that is imbedded within the larger OL-PZ, in Figure 3. It is this residual stress that leads to the delay cycles (Figure 3 insert) and further affects the crack extension. If the PZ is a measure of the deformation field, the difference between the OL-PZ and the PZ at K_{base} can be considered as a measure of residual stress (K_{res}) exerted by the OL-PZ on the newly formed PZ at K_{base}. This K_{res} is compressive due to OL being tensile and can be written as $K_{res} = f\{(PZ)_{OL} - (PZ)_{base}\} = f(\text{Excess-PZ})$, indicating K_{res} is proportional to Excess-PZS. This part has been discussed in our earlier article by Vasudevan and Sadananda (2011).

It is observed that during the Post-OL region there is a significant reduction in (da/dN) that can be close to the threshold (da/dN). The insert in Figure 3 shows a fractography of a 7075-T6 alloy in lab air before and after OL sequence showing that the ductile dimple fracture in the CA region has changed to near-threshold flat fracture (after OL), due to a reduction in maximum stress intensity (K_{max}) such that applied cyclic stress intensity ΔK_{app} (~9 MPa(m)$^{1/2}$) is close to the $\Delta K_{th} = 2.6$ MPa(m)$^{1/2}$ in the lab air. The change in fracture mode in the Post-OL part appears to be like near-CA threshold fracture without an OL. The top right-hand insert shows the delay cycles during Post-OL region and the crack length "a" vs. cycles N_d that persist until the crack has propagated out of the OL-PZ. This retarding force on the crack tip is more than the CA-PZ, and it is the excess PZ that is considered as the effect of a residual stress on the Post-OL crack growth.

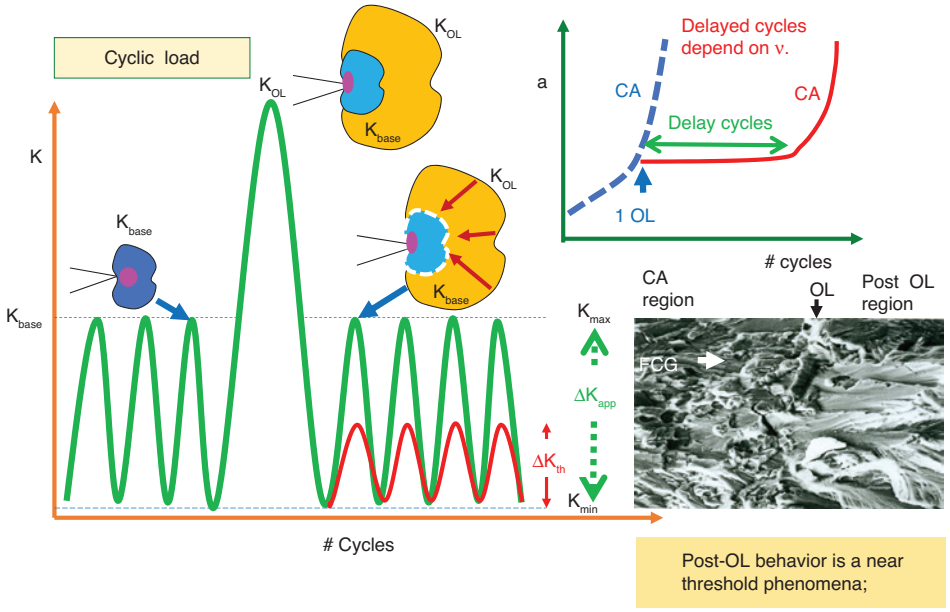

Figure 3: Schematic drawing showing the changes in the PZS during CA loading, single OL and followed by CA. Inserts show a fracture surface before and after a single 100% overload and the delay cycles due to overload.

4.2 Method of calculating residual stress intensity K_{res}

Schematics in Figure 4 show the steady state CA crack growth behavior for a given load and environment. This CA-FCG result is taken as our reference curve. Any deviation from this reference state is considered as due to an additional perturbation on the steady state stress. Thus, the application of an OL at a given applied K_{max} perturbs this steady state CA behavior. The difference in the driving force between Post-OL and CA curves, taken at a constant (da/dN), is a measure of the residual stress ($K_{residual} = K_{res}$). Thus, $K(res) = K(OL) - K(CA)$ estimated at the same (da/dN). These OLs affect the monotonic plastic zones (PZ) and thus affect the local K_{max} value than ΔK. These are maximum stress intensity values that can vary with (da/dN) and the crack length and can be plotted as such. The minimum in FCG rate in Figure 4 gives the maximum K_{res}. Crack length and load was measured in the Post-OL + CA region and plotted as K versus crack extension. These two methods gave similar results. Unfortunately, there is no *direct independent* approach available to quantify K_{res} and verify the above method. One can use finite element method (FEM) to calculate K_{res}, and this method also involves some assumptions. Reference to CA threshold $K_{max,th}$ is shown in Figure 4.

There are many types of "internal stresses" and their sources that can affect fatigue damage, and these have been discussed in detail by Vasudevan et al. (2001). In the present case, residual stress is considered as a subset of

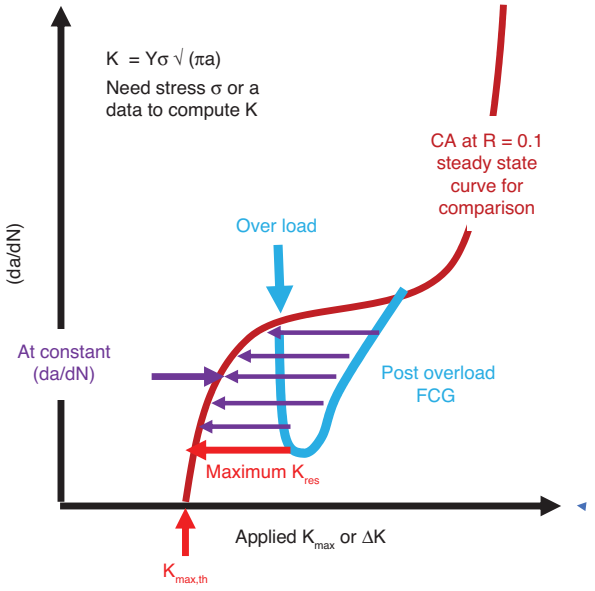

Figure 4: Method of estimating the Post-OL residual stresses by subtracting the Post-OL applied stress intensity K_{max} from the CA at the same (da/dN). By repeating this process, we can plot $K_{residual}$ (K_{res}) vs. crack extension. The minimum in (da/dN) gives the minimum residual stress. $K_{res} = K(OL) - K(CA)$ at the same (da/dN).

the *general* internal stress source. The following list gives a few examples of internal stress:

1. If there are two cracks or any two defects, the interaction force between them is the force due to internal stress.
2. Residual stresses due to deformation or rolling or shot peening are sources of internal stresses as they exist even after the external stresses are removed.

3. Stresses arising from deformation incompatibilities in composites, second-phase precipitate microstructures and hard or soft inclusions are all internal stresses.
4. Any stress gradient becomes a source for internal stresses.
5. Equilibrium condition demands that the total force due to all internal stresses must be balanced and is equal to 0.

Figure 5A presents a set of experimental data showing the variation of K_{res} with the crack extension Δa, on a linear plot. K_{res} was calculated using the method (load-Δa), described in Figure 4. The data compares results for the vacuum and NaCl environments for Types-A and B shown in Figure 1C. The scale is in negative numbers since these are all compressive stresses due to tensile OL application. K_{res} is high at low Δa and decreases with increase in Δa as it approaches the steady state CA condition, where $K_{res} \rightarrow 0$. It is interesting to observe the K_{res} persists past the OL-PZS of ~420 μm (=0.00042 m) for Type-B condition. Calculated OL-PZS (~420 μm) for applied $K_{base} = 7.9$ MPa(m)$^{1/2}$ is shown for the vacuum and NaCl (Type-B) environments. For Type-A, the OL-PZS (~52 μm) is small due to lower $K_{base} = 2.8$ MPa(m)$^{1/2}$. OL-PZS is calculated using the equation $r = 0.03(K_{OL}/\sigma_{ys})^2$. The corresponding Excess-PZS are 390 μm for Type-B and 49 μm for Type-A. Refer to Figures 1C and 2A for the legend. These OL-PZS remain constant during Post-OL CA cycling. Several specific observations can be seen in Figure 5A for the three environments:

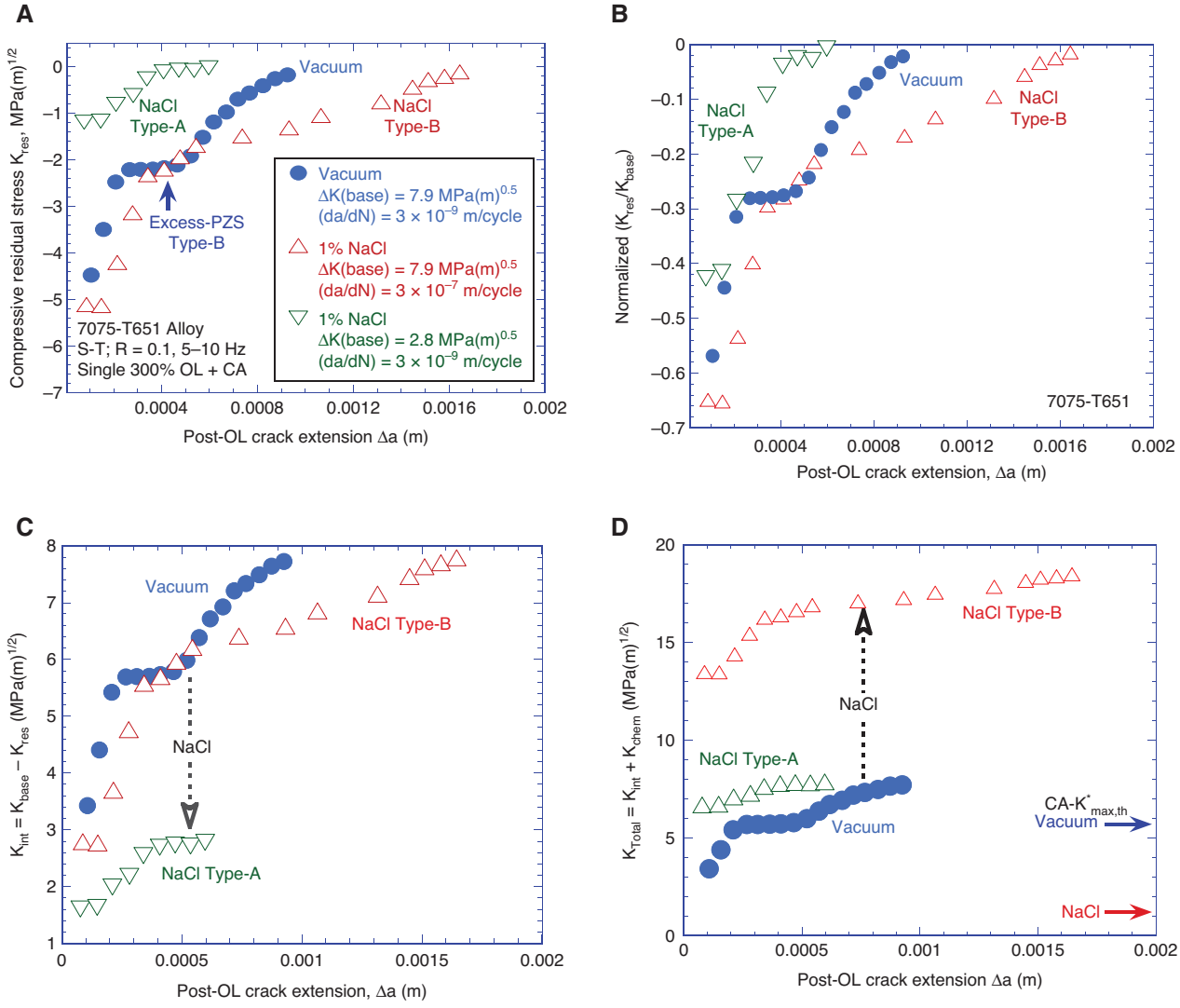

Figure 5: (A) Compressive K_{res} variation with Post-OL crack extension CA loading, for the vacuum and NaCl for Types-A and B behavior; (B) normalized variation of the data in (A) by K_{base} for the same three environments; (C) $K_{int} = K_{base} - K_{res}$, variation with crack extension and (D) crack tip $K_{total} = K_{int} + K_{chem}$, variation with crack extension Δa.

1. K_{res} decreases with increase in Δa for all three cases in the Post-OL region with CA cycling; the shapes are similar.
2. At $K_{res} - \rightarrow 0$, Δa for the vacuum reaches ~900 μm, for Type-B Δa ~1700 μm and for Type-A Δa ~500 μm; the small plateau in the vacuum data is unclear, possibly due to the crack trying to get past the excess-PZ region.
3. For Type-B, where applied K_{base} (=7.9 MPa(m)$^{1/2}$) is fixed, K_{res} decreases with Δa are large when Δa < 450 μm for the vacuum and NaCl environments. Here the K_{res} is inhibiting the K_{chem} effect in growing the crack until the excess PZ is reached where K_{chem} contribution is helping further crack extension, as NaCl is increasing with Δa. Thus, the change in the kinetics of the environmentally induced crack growth is shown in Type-B as an additional increment in the crack growth due to the superimposed environmental contributions. K_{res} then decreases with a lower slope with the crack length when Δa > 450 μm. At small Δa larger compression stress is affecting the growth where the crack is within the OL Excess-PZ region, and at higher Δa where compression stresses are decreasing, NaCl is adding to the kinetics of growth since K_{chem} is increasing with the crack growth rate resulting in the crack extension Δa. In this Post-OL region, the applied $K_{base} > K_{Iscc}$ and K_{chem} is increasing with FCG rate, suggesting that corrosion process superimposed on mechanical fatigue is becoming important; the transition in K_{res} for Type-B occurs around the Excess-PZS ~ 400 μm.
4. For Type-A, where the crack growth rate (da/dN ~ 10^{-9} m/cycle) and K_{chem} is constant, K_{res} variations with Δa are small in the Post-OL region due to lower applied K_{base}. Here the applied $K_{base} < K_{Iscc}$ and the environmental SCC effect is less. The near-threshold time-dependent corrosion fatigue process becomes important to give true corrosion fatigue. Compression residual stress is decreasing the applied K_{base} to extend Δa in this region.

When the K_{res} was normalized with respect to applied K_{base} for all three cases and plotted against Δa (Figure 5B), the overall trend did not change much. The legend for Figure 5B is given in Figure 5A. The effect of K_{res} changes is *mostly* due to NaCl contribution. At Δa < 400 μm the two environmental results tend to collapse with the vacuum data, at lower crack lengths. This could be due to the compressive residual stress suppressing the crack extension at low crack lengths when the crack is extending through the PZ and NaCl is adding to the decreasing K_{res}. In this region, the reduction in K_{res} is rapid for all three environments until it reaches the Excess-PZS quickly, and as Δa > 400 μm the crack extension rate slows down. Once the crack has passed the Excess-PZS around 400 μm, the combination of NaCl and relaxation of stresses by Post-OL CA loading may be affecting the gradual decrease in K_{res} with Δa. Interestingly, Type-A result is above the vacuum result, and Type-B is less than the vacuum result. It can be due to the applied driving force being reduced more for Type-A by NaCl relative to Type-B. These trends are reflected in the role of internal stress with Δa which is discussed in Figure 5C.

Figure 5C gives the summary of data converted from Figure 5A to present in the form of internal stress K_{int} variation with Δa. We have defined internal stress as $K_{int} = K_{base} - K_{res}$ (Vasudevan & Sadananda, 2011). Figure 5C shows the variation of K_{int} with Δa for the three environments. The overall trend is similar for all three cases, and the two NaCl results show lower K_{int} compared to the vacuum. Here we can observe that K_{int} is largely affected for Type-A by NaCl over the entire Δa length than for Type-B. This is because the growth is mainly due to Post-OL CA cycling, since the crack has passed the Excess-PZS ~49 μm. The NaCl reaction can be relieving the residual stresses chemically to affect K_{int}. For Type-B case, K_{res} is suppressing the growth (Figure 5A) as the crack is moving through the Excess-PZ with a smaller effect from the NaCl reaction at the crack. When the crack has passed the Excess-PZ the growth is slower for Type-B with a decrease in K_{int} at higher Δa.

Figure 5D shows the trend in behavior in terms of the total crack tip stress $K_{total} = K_{int} + K_{chem}$ with Δa. K_{int} is taken from Figure 5C, and K_{chem} is larger for Type-B (10.7 MPa(m)$^{1/2}$) than for Type-A (5.1 MPa(m)$^{1/2}$) for CA loading. Using Post-OL FCG data (not shown) (da/dN)-K_{max}, we find that chemical contribution for Type-A is constant but increases with Δa. For comparison the intrinsic CA thresholds ($K^*_{max,th}$) for the vacuum and NaCl are shown. Since the crack growth is possible only when $K_{total} > K^*_{max,th}$, the growth is observed at all Δa for the two NaCl results and in the case of the vacuum the growth occurs only when the crack leaves the Excess-PZ ~400 μm. Type-A results are close to those in the vacuum suggesting residual stress is affecting the K_{total} with less effect from NaCl. Type-B results are much higher than those in the vacuum suggesting NaCl contribution to K (K_{chem}) is increasing with Δa. The legend for Figure 5B–D is listed in Figure 5A.

Croft et al. (2007) for the same 300% OL conditions in a 7075-T651 as Type-B at the same $K_{base} = 8$ MPa(m)$^{1/2}$ mapped the strain-distance profile at mid-thickness of a CT sample, using synchrotron radiation and estimated the PZS for the three environments (vacuum, lab air and 3.5%

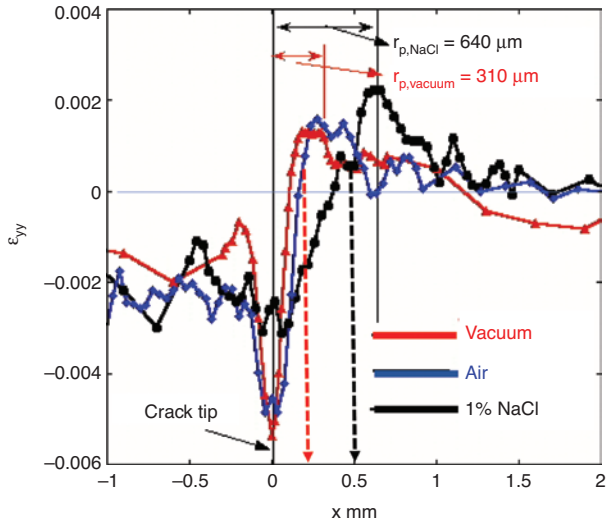

Figure 6: Synchrotron XRD strain profiles (7075-T651 alloy) for Type-B condition for the vacuum, air and NaCl environments with a single 300% overload followed by CA loading. Data taken from Croft et al. (2007).

NaCl), shown in Figure 6. Their PZS values for NaCl were about twice that for the vacuum, like the one shown in Figure 5A. Croft's OL-PZS measurements are comparable to the calculated PZS; for the vacuum it is about 310 µm vs. 420 µm (for Type-B). The measurement for NaCl was about 640 µm. We have no calculation for PZS in NaCl. Indirectly, Figure 5A shows that the ratio of Post-OL PZS ratio vacuum to NaCl is about 2, which is what Croft et al. (2007) also measured. Their measurement also shows that in the vacuum the crack tip normal strain ε_{yy} is lower than in the NaCl environment, depicting the large reduction in OL-(da/dN) in the vacuum compared to that in the NaCl environment. This observation may be due to the lowering of the lattice friction stress in NaCl to extend the PZS further under the Post-OL CA cycling region. NaCl may be reducing the friction stress to sharpen the crack tip more than in the vacuum. The characterization the OL experimental results in terms of residual stress are discussed in the next section using the modified Kitagawa diagram.

5 Results and analysis

It is observed that residual stress can vary with many factors discussed by Suresh (1998) and Sadananda et al. (1999):

1. applied stress or K_{base} from which an OL is applied and load ratio;
2. OL ratio;
3. with environment like the vacuum or NaCl;
4. OL retardation delay cycles;
5. PZS;
6. crack length; and
7. crack growth rate.

In the present study we only examine the role of Post-OL crack growth on the crack length, for a 7075-T651 alloy in the vacuum and NaCl environments for the Types-A and B experiments described in Figure 1B. This type of analysis directly relates to the Kitagawa plot which can be used to explain the Post-OL crack growth phenomenon.

5.1 Residual stress σ_{res} vs. the crack extension

In order to comply with the Kitagawa format, K_{res} in Figure 5A is converted to stress by using $\sigma_{res} = (\pi \cdot \Delta a)^{1/2} K_{res}$ since the crack length data was available. Figure 7 shows the residual stress σ_{res} profiles as a function of Δa in log-log coordinates for the two NaCl environments using the vacuum as the reference, in the Post-OL crack growth region. This figure is plotted for a single 300% OL, and the values are in *positive* numbers even though they are compressive stresses. σ_{res} is decreasing with Δa for all three cases. They are all mechanical stresses showing the effect in different environments. The data is for both Types-A and B behavior compared to the vacuum results. The trends are similar to a gradual decrease of σ_{res} until the crack has passed the OL-PZS ~420 µm and then decreases further rapidly to merge with the CA results. The rapid

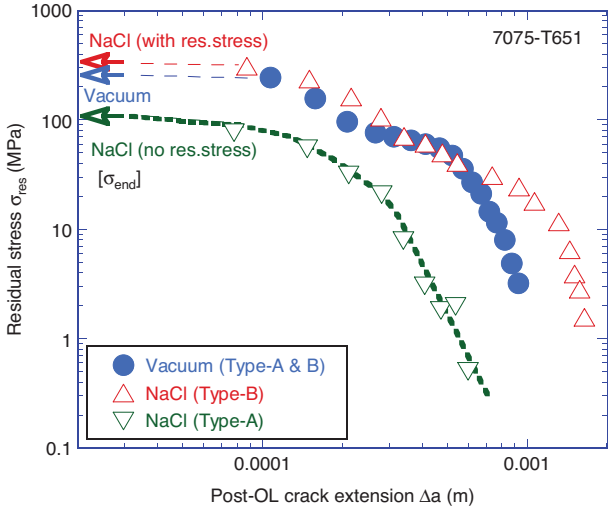

Figure 7: Compressive residual stress profiles $\sigma_{res} - \Delta a$ for the three environments shown with reference to fatigue limits. For reference, constant amplitude endurance limit values are shown.

decrease in σ_{res} is due to the crack having left the OL-PZS and the residual stress effect is reducing under continued CA loading. Reduction in σ_{res} for Type-A is due to lower K_{base}, and the increased σ_{res} is due to higher FCG rate in NaCl for Type-B. Thus, the effect of the chemical environment is affecting σ_{res} during the crack extension in different magnitudes under the same compression stress field for Type-A vs. Type-B. In all three cases, the crack is gradually transitioning from compression to tension where the Post-OL crack approaches the steady state CA. The variation in the σ_{res} trends is due to

1. compression stress due to the application of OL;
2. crack tip chemistry affected in the compression field; and
3. Post-OL CA tension cycling relaxing the OL compressive stresses with the crack extension.

In addition, the NaCl contribution for Type-B is higher compared to Type-A since the K_{chem}(Type-B) > K_{chem}(Type-A). For comparison, the endurance limit in the vacuum and in NaCl with/without residual stress (Prevey & Cammett, 2004; Lee et al., 2009) are shown. All three σ_{res} curves at low Δa approach the corresponding endurance limits.

Figure 8 converts the $K_{total} = K_{int} + K_{chem}$ data in Figure 5D into total stress σ_{total} using the relation $\sigma_{total} = K_{total}/(\pi \cdot \Delta a)^{1/2}$. Results are plotted in log-log coordinates. σ_{total} decreases with the crack extension Δa for the vacuum and both NaCl results. This gives the Kitagawa plot for all three cases, with the Kitagawa slope of about 0.4. There is some deviation at low and high crack lengths for the vacuum result which is unclear. Addition of NaCl seems to add to the total stress increasing the crack tip stresses

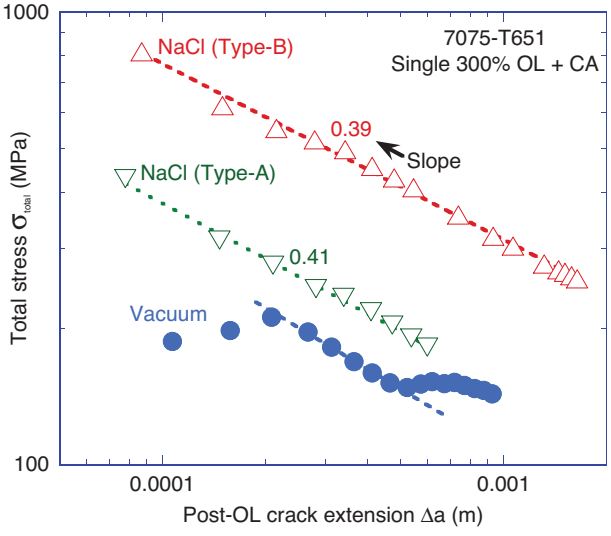

Figure 8: Total stress profiles σ_{total} – Δa for all three environments converted from Figure 5D showing the Kitagawa plot.

and indicating that the blunt vacuum crack may be sharpened by NaCl. At a constant Δa, σ_{total} is increased for both Types-A and B, or at a constant σ_{total} Δa increases. It is possible that for both Types-A and B the crack tip mechanism could be that NaCl is reducing the driving force in Type-A and NaCl is affecting the kinetics in Type-B. In both cases, residual stress is affecting the material resistance depending on the background applied K_{base}. NaCl can be affecting more in Type-B by sharpening as the crack advances to increase the crack tip stress more compared to Type-A. The details of the crack tip mechanism are unclear at this stage; hydrogen assisted cracking (HAC) type mechanism can be assumed.

5.2 Kitagawa diagram

OLs cause excess plastic zones to be higher than the steady state plastic zone. Plastic zone, in terms of constituent dislocations, contributes to the backward force on the crack tip that must be overcome for the crack to move forward. This backward force becomes one of the major contributing factors for the crack growth resistance. At the threshold condition, it forms the major factor in determining the $K_{max,th}$ value. With increasing crack growth rate, K_{max} increases with increasing crack length and correspondingly the PZS also increases establishing some steady state value.

When a single OL is applied in one cycle during a steady state growth of a crack and the specimen is recycled again at the CA, the OL creates an excess plastic zone consisting of many dislocations which exerts excess backward force on the crack tip above the steady state value. This is normally considered as compressive forces due to residual stresses introduced by the OL. The plastic zone exerts a retarding force when it is ahead of the crack tip and not when the zone moves behind the crack tip, as shown earlier in terms of the dislocation-crack interactions (Sadananda & Ramaswamy, 2001). Since the specimen is being cycled at the background steady state amplitude, the crack tip experiences a resultant tensile force due to the background amplitude contributing to the crack growth and the compressive forces due to OL plastic zone retarding the crack growth. One can measure the effective compressive force due to the OL plastic zone using (da/dN)-K_{max} curve by invoking the similitude concept that says equal crack tip forces contribute to equal crack growth rates. If the crack length data is available after OL, then one can determine the compressive residual stress using the compliance relation (shown in Figure 5A). Figure 4 is replotted as Figure 9A to complement Figure 9B.

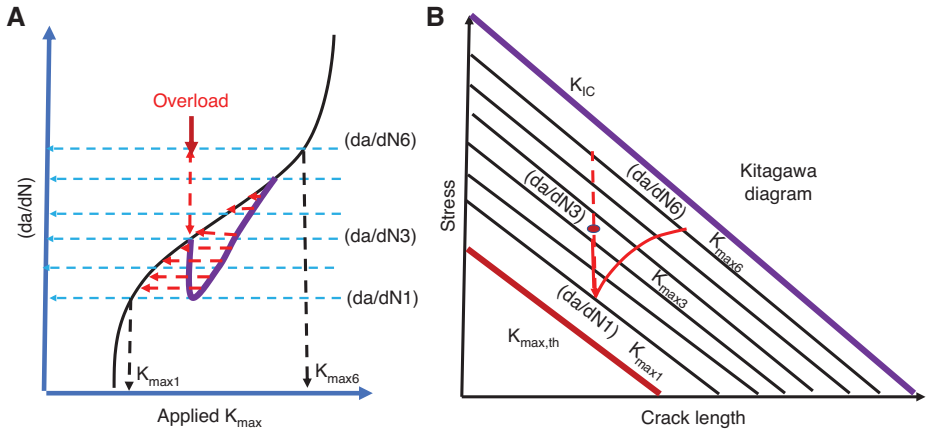

Figure 9: (A) Schematic interpretation showing the single overload and post overload crack growth rates in relation to the background constant amplitude (da/dN)-K_{max} curve. The effect of the overload residual stresses affecting different levels of (da/dN)/K_{max} is described; (B) the profile of residual stresses variation with K_{max} on a Kitagawa diagram.

A Kitagawa diagram, described by Kitagawa and Takahashi (1976), can be used to illustrate the effect of the OL based on total effective stress and the relative residual stress. This is shown in Figure 9A and B. An initial OL is applied at (da/dN)3. At the peak OL, the crack growth rate corresponds to (da/dN)6 and the correspondingly K_{max6} will be the imposed driving force. If the specimen is cycled at that amplitude, then the crack grows rapidly contributing to failure. However, if the OL is released and the specimen is brought back to the background CA, then the crack does not grow at the original rate due to reduction in the crack tip driving force, and it now grows much slower depending on the OL ratio. Based on the crack growth rate, we can determine the effective applied driving force due to the superimposed excess plastic zone. As the cycling continues, the one-time-generated excess plastic zone will get slowly affected by the newly generated plasticity. As the crack tip slowly comes out of the OL plastic zone which is continuously getting modified, the net stress slowly changes back to the background value. Based on the crack growth rate value, we can determine the effective crack tip driving force, and using the background steady state crack growth rates, we can also determine the profile of the compressive stress that is slowly changing with continuous background cycling. The profile is schematically shown in Figure 10.

Thus, the modified Kitagawa diagram, described by Sadananda et al. (2017) and Sadananda and Sarkar (2013) can be used to represent how the compressive stresses during OL retardation can be analyzed. Figure 11 is a schematic relation between applied stress "σ" and crack extension "a" on a log-log plot. Applied stress "σ" can be calculated from Figure 5 by using the relation $K_{res} = \sigma(\pi a)^{0.5}$.

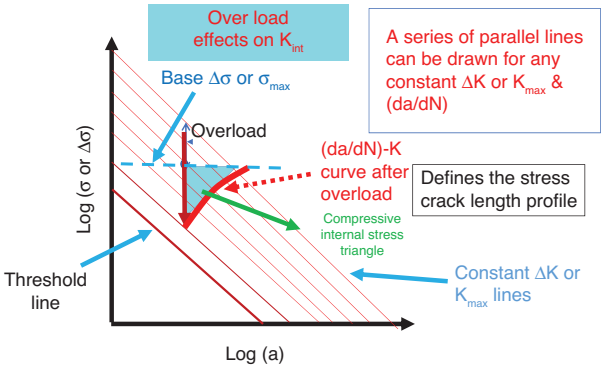

Figure 10: Use of modified Kitagawa plot to represent the compressive internal stress during overload retardation in Figure 8. This is like Figure 9B with details of inverted internal (residual) stress triangle.

One can then draw a series of parallel lines representing K_{max}. For reference, base stress "σ_{base}" is shown where the OL is applied resulting in a compressive residual stress. The crack growth occurs in the compression field by cutting across many of these constant K_{max} lines until it reaches the failure at K_{1c}, giving an inverted "internal stress" or "residual stress" triangle. If NaCl is imposed on such a profile, then an additional effect modifies the compressive stress to further change the crack tip stresses, as in Figure 10.

5.3 Crack chemistry

Crack tip chemistry and its reaction rates are governed by local open circuit potential E_{OCP} and pH. There is a large body of articles written on crack chemistry under fatigue

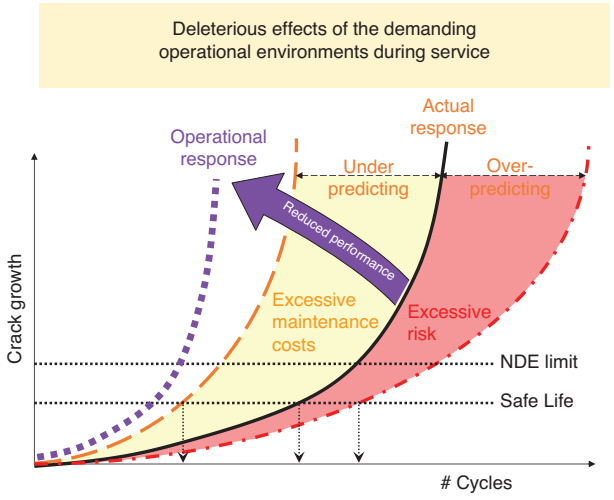

Figure 11: Schematic illustration to show the deleterious effects from the demanding service environments (load and chemistry) on the component life due to overload and underload. Navy NDE and Safe Life limits are also marked for reference.

loading with applied potential varying from the anodic to cathodic range. There is not much work done on crack chemistry under an applied variable loading in fatigue when the crack tip opening displacement is varying and with no applied potential. Wei (2010) has discussed some key steps involved in the environmental process:

1. bulk transport of NaCl to the crack tip to form passive oxide;
2. chemical reaction rate that can dissolve the oxide and produce damaging ions that can adsorb to the crack surface; and
3. changing the crack tip E_{OCP} and pH.

All the mechanisms require a discrete set of chemical reactions to occur for cracks to grow. The rate-determining step of a mechanism would be the slowest step in the sequence of reactions required by the mechanism. Due to the similarities of the different mechanisms, there are only a few specific possible rate-determining steps for a given fracture event. Critical experiments with analysis on the role of compression stress on the crack tip chemical reaction is lacking. Prevey and Cammett (2004) have measured polarization curves on cold rolled 7075-T651 plate. Their result indicated that there was a decrease in E_{OCP} (~0.12 V, SCC) and a small increase in current with increase in percent cold work. They implied that cold work increased the electrochemical activity resulting in greater propensity to corrode at a faster rate. Most of the corrosion damage was in the form of pitting.

Qualitative experiments done by Kujawski and Sadananda (2011) under a static compression stress at a notch, showed that the chemical reaction can be reduced or delayed until the crack has extended beyond the compression PZS. No electrochemical data was recorded.

In addition, cyclic deformation can modify the chemical reaction rates at the crack tip affecting the local plastic behavior. This is shown to be the case for CA cycling (Turnbull, 2001). This can be manifested in terms of anodic reaction leading to metal dissolution or cathodic reaction with hydrogen evolution. The reaction rate is controlled by the time the bare metal is exposed during cycling. Analysis becomes difficult as there are many electrochemical reactions, for a given NaCl composition, at the crack associated with mass transport of the bulk NaCl solution and its thermodynamics that govern the reaction rates. The solution chemistry at the crack can be very different from the bulk in terms of pH, ionic species, oxide formation etc. It is the stability of the oxide film and subsequent exposure of new surfaces that affects a crack to extend. While complexities are being recognized, we find that the two cases in NaCl (Types-A and B) under this study can shed light on some understanding:

1. Residual stress K_{res} (and σ_{res}) contributed to the local internal stress.
2. Chemistry adds to K_{res} affecting the crack extension.
3. NaCl adds to the total crack driving force for both Types-A and B conditions (Figure 9).
4. Residual stresses are nonlinear with the crack extension (Figure 5).
5. Post-OL crack extension at $\Delta a >$ Excess-PZS is mostly governed by CA loading that can be relaxing the OL stresses as the crack extension progresses.

5.4 Implications

During service, the loads can vary randomly from tension to compression. Such variations in loads can be represented in terms of the variations in the internal stresses that can modify the K_{max} term in the life prediction equation.

These internal stress patterns can vary from cycle to cycle depending on the magnitude of the tension and compression loads, such that the K_{max} at the growing crack tip can be high or low. This in turn will affect the rate of crack growth by either retarding or accelerating it. The growth law based on CA can be used to predict the life under variable loads if the changes in K_{int} can be measured or computed for the given loading pattern.

In the final analysis, the overall connection of the required driving forces ΔK, K_{max} and the internal stress contribution to K_{max} ($K_{int,max}$) to the fatigue damage should be used to make a *reliable* life prediction model, in conjunction with FEM analysis. The overall model does require a correct representation of the service loads and how the load-load interactions can be brought together in terms of the $K_{int,max}$. It should also consider the variations in the environmental effect on the $K_{int,max}$. In the minimum, the long and short crack data should be generated at least for minimum and maximum load ratios, $R = 0.1$ and 0.9. Any single R-ratio data is *insufficient* for use in the predictive model and can lead to erroneous understanding of the damage and its use in the formalism of the damage model. We must attempt to *quantify* the non-destructive evaluation (NDE) results from the maintenance service that can be incorporated into the overall prediction model to map the damage from the early stages of the crack initiation to the long crack and final failure.

The safety of the component is a primary goal and is affected by two factors: (1) design and (2) usage life. For the component design one needs information on design stress such that life is contained, while for usage life how applied stress affects life. At the usage level, cracks are periodically monitored to ensure safety of the component life.

To account for the deleterious effects of the demanding operational environments of a component in service, we must develop a "unified" life prediction model like UNIGROW (Mikhevsky & Glinka, 2009). This is schematically represented in Figure 11. In service, both chemical environment and mechanical loads reduce the life of a component than just the mechanical loads. Thus, the damage life predictions must be well delineated to achieve the goals. The goal is to develop the predictive relations between the environment (concentration and type of chemistry) and the material (flow properties and internal/residual stress state) so that catastrophic failures can be minimized or avoided. We can then extend the predictive capability to the changing loads spectra and changing environmental conditions during service. A reliable life prediction damage model needs use inputs from (1) corrosion that affects a crack to initiate and grow with superimposed mechanical loads and (2) changing environments coupled with changing load spectra during the operational service.

In service, damage observed of a component may not arise from a single mechanism but from a combination of SCC, pure mechanical fatigue and corrosion fatigue. We note that a reliable fatigue life prediction under service loading is a challenge due to complexities and uncertainties in the material fatigue and fracture properties, mechanical and environmental loading response and surface conditions and treatment. Some of these uncertainties can never be reduced drastically but can be reduced enough with a better understanding of the nature of physical and chemical processes to a level that we can contain them. Challenges still exist in developing that one reliable model that can predict the total life for crack initiation and growth.

6 Summary

Application of a tensile OL introduces compressive residual (internal) stresses ($-K_{res}$) which affects the damage behavior under Post-OL cyclic loading conditions.

- K_{res} for the vacuum and NaCl (Types-A and B) with superimposed OLs are estimated using the corresponding steady state CA data as a reference state at $R = 0.1$.
- In all three cases, namely, the vacuum and Types-A and B, K_{res} decreases with Post-OL crack extension.
- Total stress (σ_{total}) increases with the addition of NaCl (Types-A and B) compared to that in the vacuum.
- Post-OL mechanism is mostly governed by CA loading at $\Delta a >$ OL-PZS where a small amount of residual stress remains.
- It seems that the role of compressive residual stress and NaCl effects on the crack extension may be synergistic making it difficult to decouple the individual effects on the crack extension.
- One can assume that HAC may be a mechanism for the trend in behavior. The precise role of HAC is unclear.
- In both cases, the crack tip chemical reaction rates can be affected to a different degree by the compressive stresses that affect the crack extension rate.
- The overall retardation can be described by using the modified Kitagawa diagram with an "inverse" internal stress triangle.
- For a given alloy, such observation can vary with applied K_{base}, magnitude of OL application and the surrounding chemical environment.
- For cyclic load test a crack will grow if

$$K^{Total}_{max} = K^{App}_{max} \pm K^{Int}_{max} + K^{Chem}_{max} > K^{\star}_{max,th} \text{ for long crack.}$$

  K_{total} (and σ_{total}) is higher for both Types-A and B conditions in NaCl compared to the vacuum.
- Experiments done at low frequency (<0.01 Hz, for 7075 alloy) in the Post-OL region can help understand the time effects on corrosion fatigue damage compared to cycle dependent.

Acknowledgments: AKV would like to thank Dr. Eun Lee, NAVAIR (retired) for helpful technical discussions. Thanks to Dr. N. Apetre (NRL) for increasing the resolution of the figures.

References

Chanani GR. Retardation of fatigue crack growth in 7075 aluminum. Met Eng Quart 1975; 15: 40–48.

Chanani GR. Effect of test frequency on the retardation behavior of 7075-T6 and 2024-T8 alloys. Int J Fracture 1976; 12: 652–659.

Chanani GR. Investigation of effects of saltwater on retardation behavior of aluminum alloys. ASTM STP-642 1978: 51–72.

Croft MC, Jiswari NM, Zhong Z, Holtz RL, Sadananda K, Skaritka JR, Tsakalakos T. Fatigue history and in-situ loading studies of the overload effect using high resolution X-ray strain profiling. Int J Fatigue 2007; 29: 1726–1736.

Dowling NE. Mechanical behavior of materials. New York, NY: Prentice Hall, 1993: 295.

Kitagawa H, Takahashi S. Application of fracture mechanics to very small cracks or cracks in the early stages. In: Proceedings of the 2nd International Conference on Mechanical Behavior of Materials. Metals Park, OH: American Society of Metals, 1976: 627–631.

Kujawski D, Sadananda K. Effect of crack-tip stresses on stress corrosion cracking behavior. Metall Mater Trans A 2011; 42A: 377–382.

Lee EU, Vasudevan AK, Glinka G. Environmental effects on low cycle fatigue of 2014-T351 and 7075-T651 aluminum alloys. Int J Fatigue 2009; 31: 1938–1942.

Mason ME. Time-dependent corrosion fatigue crack propagation in 7000 series aluminum alloys. MS thesis. Charlottesville, VA, USA: Department of Materials Science and Engineering, University of Virginia, 1994.

Mikhevsky S, Glinka G. Elastic–plastic fatigue crack growth analysis under variable amplitude loading spectra. Int J Fatigue 2009; 31: 1828–1836.

Pao PS, Holtz RL. Corrosion fatigue cracking in AL 7075 alloys. Final report NRL/MR/6355-14-9582. Washington, D.C.: Naval Research Labs, December 9, 2014.

Prevey PS, Cammett JT. The influence of surface enhancement by low plasticity burnishing on the corrosion fatigue performance of AA7075-T6. Int J Fatigue 2004; 26/9: 975–982.

Sadananda K. Failure diagram and chemical driving forces for subcritical crack growth. Metall Mater Trans A 2012; 44A: 1190–1199.

Sadananda K, Ramaswamy DN. Role of crack tip plasticity in fatigue crack growth. Philos Mag 2001; 5: 1283–1303.

Sadananda K, Sarkar S. Modified Kitagawa diagram and transition from crack nucleation to crack propagation. Metall Mater Trans A 2013; 44A: 1175–1189.

Sadananda K, Vasudevan AK. Crack tip driving forces and crack growth representation under fatigue. Int J Fatigue 2004; 26: 39–47.

Sadananda K, Vasudevan AK. Review of environmentally assisted cracking. Metall Mater Trans A 2011; 42A: 279–303.

Sadananda K, Vasudevan AK, Holtz RL, Lee EU. Analysis of overload effects and related phenomena. Int J Fatigue 1999; 21: S233–S246.

Sadananda K, Vasudevan AK, Holtz RE. Extension of the unified approach to fatigue crack growth to environmental interactions. Int J Fatigue 2001; 23: 277–286.

Sadananda K, Solanki KN, Vasudevan AK. Subcritical crack growth and crack tip driving forces in relation to materials resistance. Corros Rev 2017; 35: 251–265.

Suresh S. Fatigue of materials, 2nd ed. Cambridge, UK: Cambridge University Press, 1998.

Turnbull A. Modeling of the chemistry and electrochemistry in cracks – a review. Corrosion 2001; 57: 175–189.

Vasudevan AK, Sadananda K. Classification of fatigue crack growth behavior. Metall Mater Trans A 1995; 26A: 1221–1234.

Vasudevan AK, Sadananda K, Glinka G. Critical parameters for fatigue damage. Int J Fatigue 2001; 23: S39–S53.

Vasudevan AK, Sadananda K. Role of internal stresses on the incubation times during stress corrosion cracking. Metall Mater Trans A 2011; 42A: 396–404.

Wei RP. Fracture mechanics: integration of mechanics, materials science, and chemistry. Cambridge, UK: Cambridge University Press, 2010.

Article note: AKV dedicates this article to a dear friend, Prof. David Quesnel, University of Rochester, NY, who passed away in early 2018. David was an excellent teacher and was a leading scientist in the area of adhesion and stress corrosion science.